INVESTIGATION OF BUBBLE COLUMN HYDRODYNAMICS USING CFD SIMULATION (2D AND 3D) AND EXPERIMENTAL VALIDATION

Mohammad Irani*, Mohammad Ali Khodagholi

Research Institute of Petroleum Industry, Tehran, Iran, P.O.Box 18745-4163

Abstract

This article presents the results of 2D and 3D simulations of a bubble column reactor at unsteady state conditions and low gas flow rates. The simulations have been done based on a two-fluid model with a $k - \varepsilon$ model used for turbulence modeling. The experimental data have been obtained by differential pressure transducer. To analyze the hydrodynamic parameters such as hold up of phases, a system consists of water tank and air aerated from bottom has been used. The simulations have been done based on two different approaches which were mixture and eulerian approaches. Despite the fact that these approaches lead to similar results, the convergence and stability of eulerian approach was better than mixture approach. Furthermore, the effects of gas velocity and liquid height on hydrodynamic behavior of the column have been studied. Simulation results were reasonably close to the experimental data. Gas holdup has been predicted reasonably well. Results of this study shows that simple two dimensional model can't be used in engineering calculations required in the design of bubble columns

Keywords: Bubble Column Reactor; Multiphase; CFD; Eulerian.

1. Introduction

Bubble columns are contacting devices in which gas as dispersed phase contacts liquid as continuous phase. Bubble columns can be used as reactors, in various chemical processes. The reactor used in Fischer-Tropsch process is also a bubble column [1]. The main advantages of bubble columns are the lack of moving parts, which makes their maintenance easier, high interfacial areas which leads to high inter phase mass and heat transfer, and large liquid holdup which is appropriate for slow liquid phase reactions [2]. The performance of bubble columns depend on various parameters such as geometric configuration, operating conditions such as temperature, pressure, liquid height and gas flow rate. Furthermore, analyzing the performance of bubble columns consist of lots of variables considered as internal states. The most important internal states of bubble columns are as follows:

- Gas holdup through out the column.
- Gas-liquid interfacial area.
- Interfacial mass and heat transfer coefficients.
- Bubble size distributions.
- Bubble coalescence.
- Gas velocity.
- Temperature and pressure distributions.

The lack of complete understanding of the hydrodynamics of bubble columns makes it difficult to improve their performance (particularly when they are used as a bubble column reactor) by judicious selection and control of the operating parameters. The

* Corresponding author,E-mail address: iranim@ripi.ir or mohammadirani@yahoo.com

need to establish a rational basis for the interpretation of the interaction of fluid dynamic variables has been the primary motivation for active research in the area of bubble column modeling based on Computational Fluid Dynamics (CFD) tools in the last decade [3]. Various approaches have been suggested for solving the same fundamental flow problem modeling the hydrodynamic behavior of bubble columns. This problem may be solved at various levels of sophistication. One may choose to treat both the dispersed and continuous phases as interpenetrating pseudo-continua (the Euler-Euler approach) [4, 5] or the dispersed phase as discrete entities (the Euler-Lagrange approach) [6, 7, 8]. The simulation may be done in fully transient and dynamic mode [9, 10] or only for the unsteady-state time-averaged results [11, 12, 13]. An appropriate mesh and a robust numerical solver are crucial to get accurate solutions [14]. Finally, it is highly imperative to validate the simulation results against experimental work.

The main objective of this work is to come up with a detail model for bubble column in order to find the effect of major parameters on its performance. Section 2 goes through various parts of the detail model used to study the hydrodynamic behavior of the bubble column. Validation of the developed model has been done by comparing its results for liquid velocity and gas holdup at different sections of the column with their corresponding experimental counterparts obtained based on an experimental set up described in section 3. Section 4 describes the procedure used to solve the detailed model of bubble column, it then follows by section 5 in which the simulation and experimental results have been presented and compared.

2. Experimental setup

A cylindrical bubble column, 14.5 cm diameter and 260 cm height were set up in our laboratory. All the experiments were carried out using air as a sparged gas.
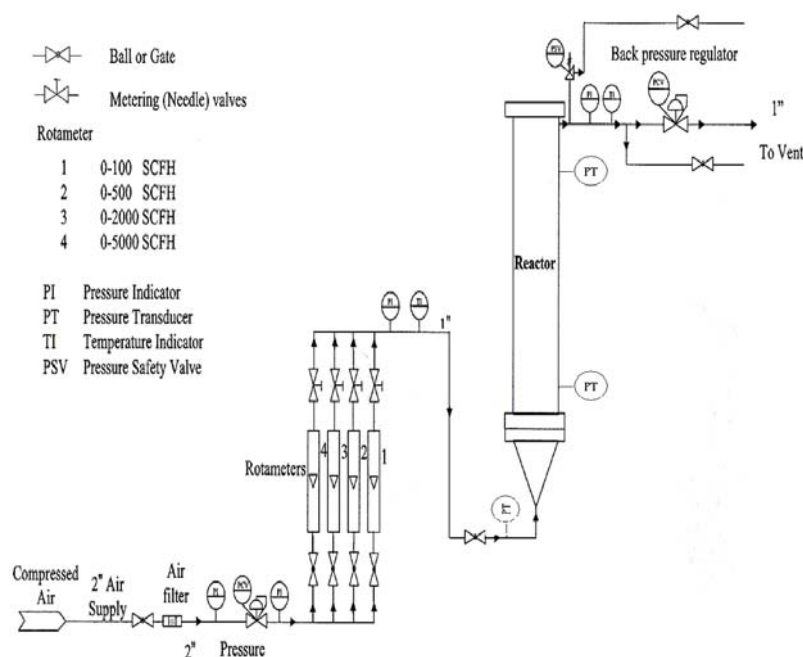

Fig.1 Schematic of experimental setup

The superficial air velocity was varied from 0.01 to 0.04 m/s. The liquid pase in the bubble column contains pure water in all the experiments. The gas is sparged in the bubble column through a Sinter glass type of sparger. Experimental studies have been done at various ratios of liquid height to column diameter (e.g., 8, 10 and 12). Two pressure transducers were used (PCB Piezotronics Inc, USA, and Model 106B50). Figure 1 shows the experimental setup used for the validation of simulation results. As seen from Figure 1 pressure sensors were flush mounted on the column.

3. Computational model

Mathematical model of the system consists of various parts which are described in the subsequent sections.

3.1. Mass conservation equation

The continuity equation describes the mass flux into and out of a control volume and the change of its mass. The continuity equation for a phase, 'q', in a multiphase flow problem is as follows:

$$\frac{\partial}{\partial t}(\alpha_q \rho_q) + \nabla \cdot (\alpha_q \vec{v}_q \rho_q) = \sum_{p=1}^{n} \dot{m}_{pq}$$

$$\dot{m}_{pq} = -\dot{m}_{qp} \qquad\qquad (1)$$

$$\dot{m}_{pp} = 0$$

The left-hand side describes the internal change of mass over time and the convective flux crossing the boundaries of the control volume. On the right-hand side the first term describes mass transfer from phase p to q and vice versa while the second term includes additional source terms. Neglecting mass transfer and source terms in Eq (1) will results in the following Eq.:

$$\frac{\partial}{\partial t}(\alpha_q \rho_q) + \nabla \cdot (\alpha_q \vec{v}_q \rho_q) = 0$$

Where α_q is the volume fraction of phase q, which needs to satisfy the relation 2.

$$\sum_{q=1}^{N} \alpha_q = 1 \qquad\qquad (2)$$

For example for a gas-liquid flow the volume fraction constraint reduces to

$\alpha_q + \alpha_p = 1$.

Equation (1) doesn't contain mass transfer since it assumed that there was no mass transfer taking place between phases , the term corresponding to this phenomenon has not taken into account in Eq.(1). This is a rational assumption, since the solubility of the air in water is very small.

3.2. Momentum transfer equations

In analogy to the mass conservation, the momentum conservation for multiphase flow is described by the Navier-Stokes equation expanded by the phase volume fraction. Such an equation for phase 'q' is as follows:

$$\frac{\partial}{\partial t}(\alpha_q \rho_q \vec{v}_{q,i}) + \frac{\partial}{\partial x_j}(\alpha_q \rho_q \vec{v}_{q,i} \vec{v}_{q,j}) = -\alpha_q \frac{\partial p}{\partial x_i} + \frac{\partial}{\partial x_j} \alpha_q \mu_q \left(\frac{\partial u_{q,i}}{\partial x_j} + \frac{\partial u_{q,j}}{\partial x_j} \right) + \rho_q \alpha_q g_i + M_{\alpha,i} \qquad (3)$$

The terms on the right-hand side describe all forces acting on the phase 'q' of a fluid element in the control volume. These forces are the overall pressure gradient, the viscous stresses, the gravitational force and interphase momentum forces combined in $M_{\alpha,i}$. The pressure is assumed to be equal in both phases. The effective viscosity

μ_{eff} of the viscous stress term consists of the laminar viscosity and an additional turbulent part in case of turbulence. The only force that has been considered so far is the drag force and the other forces have been neglected. There are various approaches that can be used for drag correlations of gas bubbles in liquid flow. In this study drag is estimated based on the correlation - 4 proposed by Clift, Grace and Weber (1978):

$$M_{\alpha,i} = \frac{3}{4} C_d \alpha_p \rho_q \frac{1}{d_b} |U_p - U_q| (U_{p,i} - U_{q,i}) \tag{4}$$

The drag coefficient was assumed to be at $C_d = 0.66$ value, while a constant bubble diameter of 3 mm was used in the simulations. The experimental observations show that bubbles diameter in the original configuration were between 1 and 5 mm.

Laminar model

In the framework of the laminar model, the turbulent effects in the liquid phase and the dispersive effects in the gas phase are neglected. Hence the effective viscosity can be obtained through the following approximation:

$$\mu_{eff} = \mu_L (1 + 2.5\varepsilon) \approx \mu_L \tag{5}$$

Turbulence equations

The flow pattern corresponding to disperse gas phase was modeled based on laminar models. The well-known single-phase turbulence model usually has been used to model turbulence of the liquid phase (as continuous phase) in Eulerian-Eulerian multiphase simulations. In the present work the standard k-ε model proposed by Launder and Spalding (1972) was used. This model is based on the following conservation equations for the turbulent kinetic energy k and turbulent dissipation ε :

$$\frac{\partial(\rho k)}{\partial t} + \frac{\partial(\rho k u_i)}{\partial x_i} = \frac{\partial}{\partial x_j}\left(\alpha_k (\mu + \frac{\mu_t}{\sigma_k}) \frac{\partial(k)}{\partial x_j} \right)$$
$$+ G_k + G_b - \rho\varepsilon - Y_M + S_k \tag{6}$$
$$C_\mu = 0.99, \ C_{\varepsilon 1} = 1.44, \ C_{\varepsilon 2} = 1.92$$

$$\frac{\partial(\rho\varepsilon)}{\partial t} + \frac{\partial(\rho\varepsilon u_i)}{\partial x_i} = \frac{\partial}{\partial x_j}\left(\alpha_k (\mu + \frac{\mu_t}{\sigma_\varepsilon}) \frac{\partial\varepsilon}{\partial x_j} \right) + C_{1\varepsilon} \frac{\varepsilon}{k} (G_k + C_{3\varepsilon} G_b) -$$
$$C_{2\varepsilon} \rho \frac{\varepsilon^2}{k} + S_\varepsilon \tag{7}$$

Where S_k and S_ε on the right-hand side of the Eqs. (6, 7) correspond to source terms describing the amount of generated turbulent kinetic energy and turbulent dissipation, respectively. Turbulent kinetic energy, as an example, can be generated by the local shear in single-phase flow, where as in two-phase flow it can be generated because of the energy associated to bubble wakes. The effective viscosity of phase q in Eq. (4) is calculated as follows:

$$\mu_{q,eff} = \mu_{q,lam} + \frac{\mu_{q,tur}}{\sigma_k}$$

Using the standard $k - \varepsilon$ model the turbulent viscosity of the continuous phase is calculated by the following equation:

$$\mu_{q,,tur} = C_{\mu} \rho \frac{k^2}{\varepsilon}$$

4. Numerical solution procedure

Fluent software was used for simulation of 2D and 3D cases. In this approach mass and momentum balance equations are solved for each phase.

The transient behavior of the bubble column exists in the experimental setup has been obtained based on the solution of its 2D and 3D mathematical models.

5. Simulation and results

5.1 Simulation results for laminar cases

We have used the RIPI experimental data in order to validate our simulation results both for gas velocity data. Figure 2, 3 shows the liquid velocities obtained based on both laminar and turbulent models and its corresponding experimental data.

Fig. 2 Velocity profile (at L/D=4) for turbulent and laminar cases

As Figure 2 shows laminar results overestimate the fluid velocity almost everywhere due to numerical diffusion of the upwind discretization. In order to reduce the effect of numerical diffusion one can decrease the grid size which leads to the increase in the number of nodes spanning the whole domain.
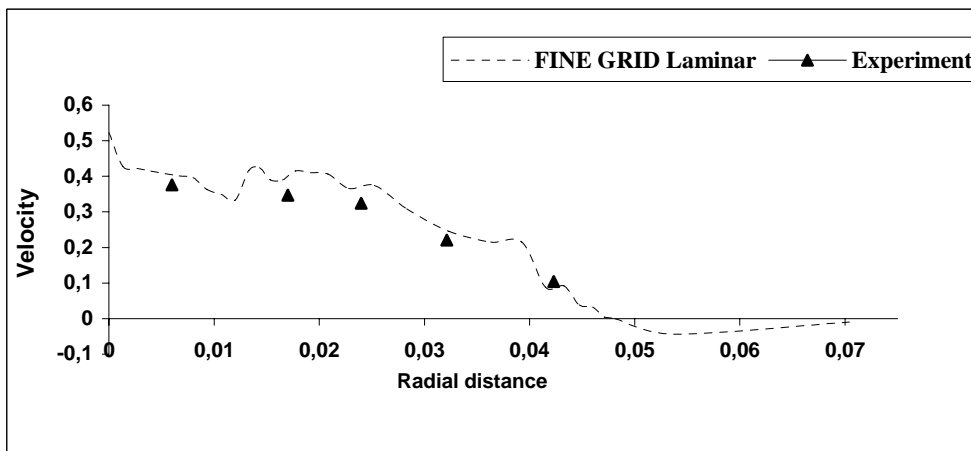

Fig.3 Velocity profile (at L/D=4) for fine grid laminar case

As shown in Fig. 3 the results of simulation based on laminar regime is closer to the experimental data for smaller grid size. This can be seen from the contours of volume faction of the system shown in Fig 4 both for course and fine grids.
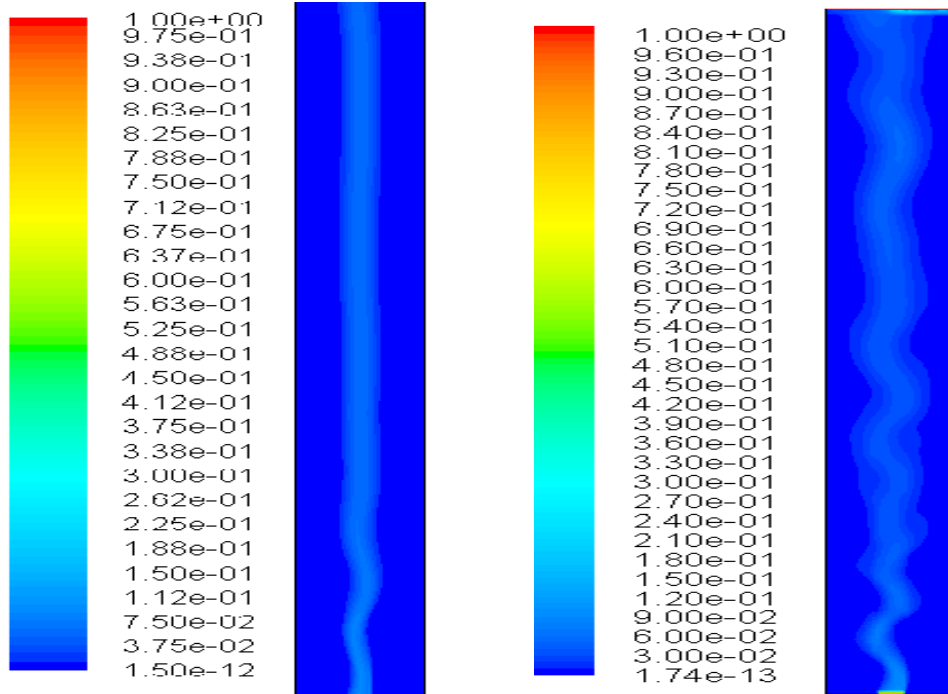

Fig. 4 Contours of volume fraction for coarse grid (left) and fine grid (right) cases

Figure 5 shows the bubble distribution obtained from the experimental setup. Comparison of these figures shows that the simulation results depend strongly on the space resolution used. The finer the grid size the more vortices are resolved, in accordance with the turbulent character of the underlying flow (Fig.5)
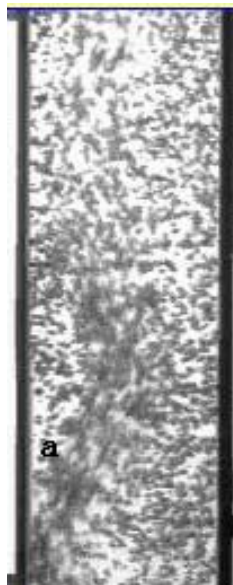

Figure5. Snapshot of set up t=30 sec

The form of the undulation, however, differs from that observed in the experimental study. In particular, the stable lower part of the bubble swarm, which is always directed against the near sidewall in the experiment was not correctly reproduced in the simulation This comparison led us to obtain the hydrodynamic behavior of the system based on turbulent assumption, this is due to the fact that based on Fig. 5 and Fig.6, and it seems that the assumption of laminar flow pattern is far from reality. In next section, the simulation results obtained based on turbulent regime is introduced.
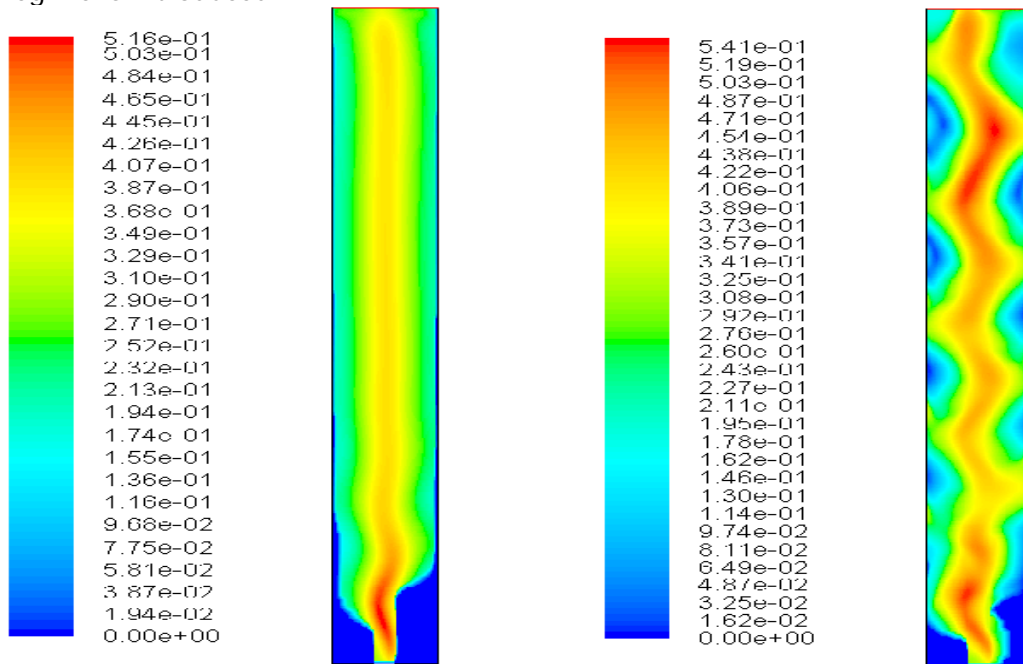

Figure6. Contour of velocity for turbulent (left) and laminar (right) cases after 30 sec

5.2 Simulation results for turbulent cases

In order to simulate the hydrodynamic behavior of the system in turbulent regime, the calculations were started with the laminar model with the liquid at rest.
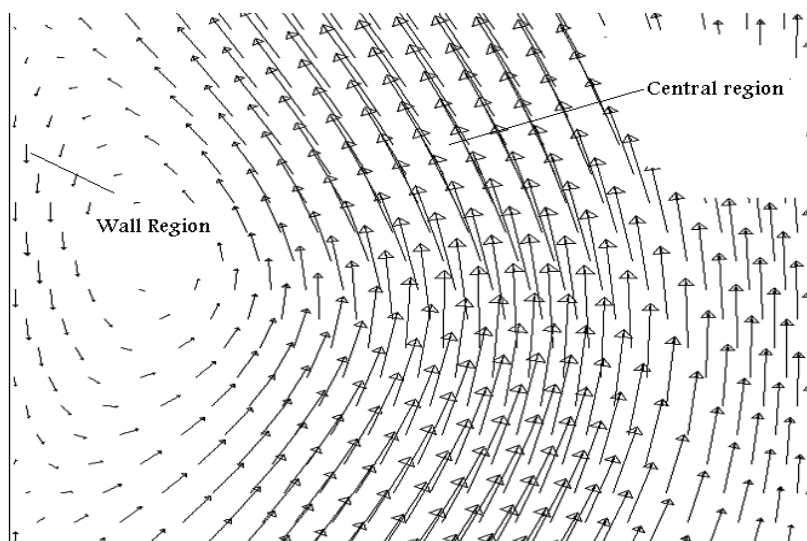

Fig. 7 Velocities vector in center and wall region of column

Some seconds after the beginning of the aeration, when the liquid velocity in most parts of the reactor was greater than zero, the k and ε fields were initialized and the turbulence model was switched on. The laminar model marks the starting point of the evaluation for the turbulent approach with a basic k-ε model. All simulations showed a qualitatively correct picture of the overall fluid circulation. We can see strong upward flow in the central region above the gas sparger and downward flow near the column walls (Fig.7).

According to Fig. 2 despite the fact that laminar results overestimate the fluid velocity almost everywhere. The turbulent model, on the other hand predicts the fluid velocity fairly accurately (Fig. 8).
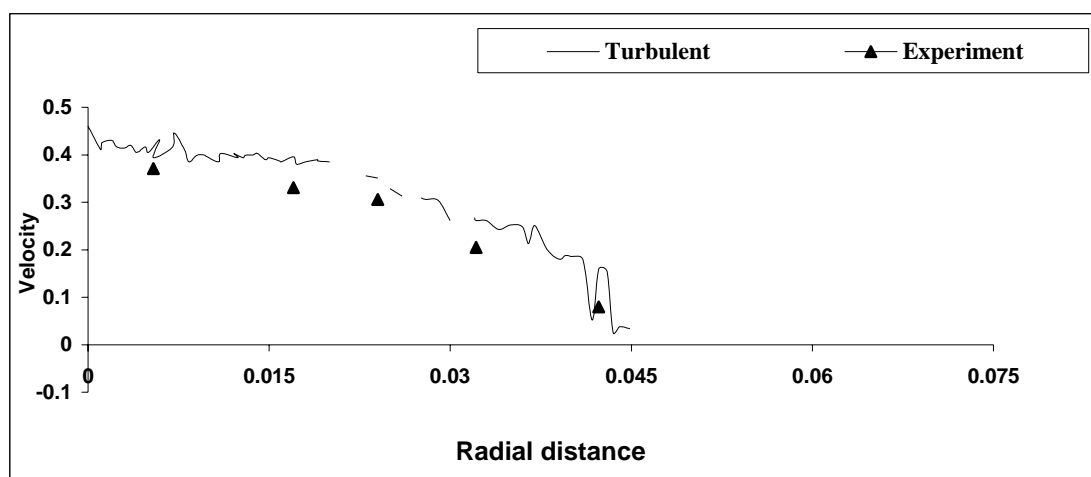

Fig. 8 Velocity profile (at L/D=4) for turbulent case and experiment

In the case of the 2D simulation with k-ε turbulence model no long-time dynamic solution can be achieved, and the changing velocity fields, presented before, are due to the transition during the start-up (Fig.9). As seen in Figure. 2, 8 the maximum value of velocities in laminar and turbulent model is the same. It is due to the fact, that the numerical diffusion of the upwind discretization has a similar influence as the turbulent eddy viscosity in the turbulence models. Gas has a meandering path.
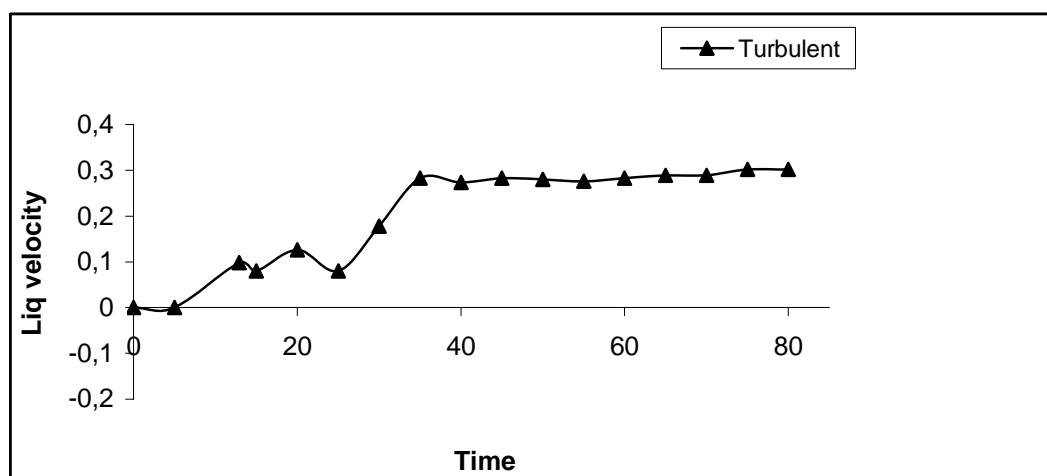

Fig.9 velocity of liquid Vs time for 2D turbulent case

The volume average of holdup for turbulent and laminar regimes was 0.022 and 0.019 respectively. In the 2D turbulent calculations the highest turbulent kinetic energy was found in the regions of the strongest changes in liquid velocities, i.e. in the central part of the large-scale vortices. Near the solid walls a strong decrease in the magnitude of turbulence intensity observed. (Fig. 10)
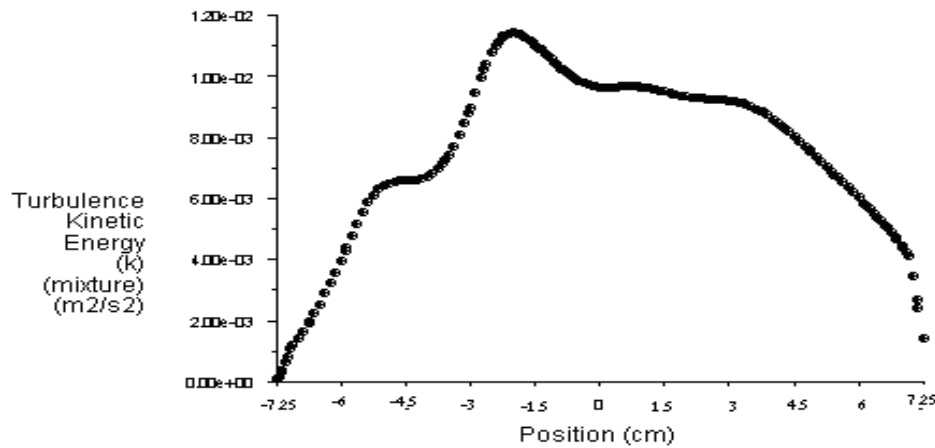

Figure.10 Profile of the turbulent kinetic energy

It is therefore obvious, that the intensity of turbulence decreases near the cylindrical wall of the apparatus which leads to lower turbulent kinetic energy inside the bubble column. This effect is completely neglected in a two-dimensional calculation, and could only be verified with a full three-dimensional model. In order to see the effect of dimension reduction in the hydrodynamic behavior of the system and due to the 3-D characteristics of turbulence, the hydrodynamic behavior of the system has been obtained based on a 3D model. The obtained results are in better agreement with experimental results.

The results of three-dimensional simulations with the turbulent Euler-Euler model show, that the front and the back walls indeed dampen the intensity of turbulence inside the bubble column, so that the turbulent eddy viscosity becomes about one order of magnitude smaller than its corresponding value one in the 2-D simulation. The overestimation of the effective viscosity in the 2-D simulation is the main reason for the fact that the time required for the system to get to its steady-state is less than what happens in reality. (Fig. 9) The details of the results obtained in 3D simulation are discussed in next section.
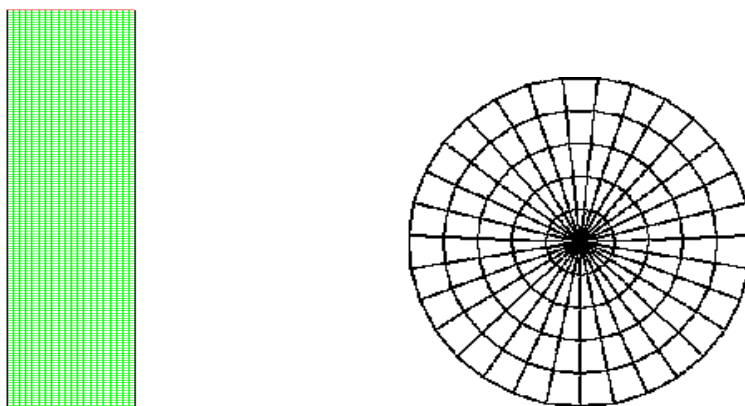
5.3 Simulation result for the 3D model

Fig. 11 Bottom and side view of meshed geometry

Fig. 11 shows the structured mesh used in the 3D simulation of the system. In order to validate the results of 3D simulation the simulated and measured total gas hold up for various inlet gas velocities are compared in Figures 12 to 16. These Figures show a very good agreement between the results obtained by 3D simulation and their corresponding measured ones.

As can be seen from Figure.12 predicted holdups for 2D and 3D cases are some how different and probably this difference is due to overestimation of turbulent viscosity in 2D case.
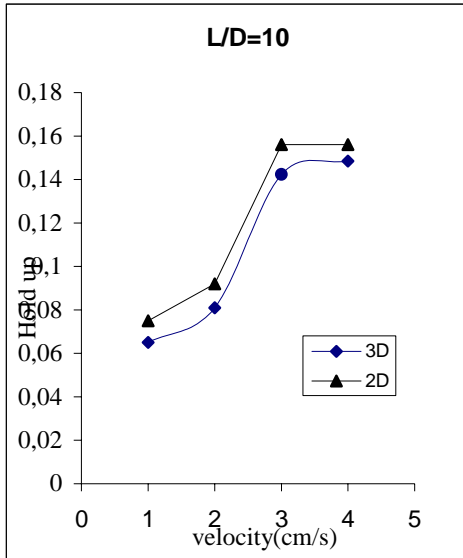

Fig. 12.Comparison of 2D and 3D gas holdup

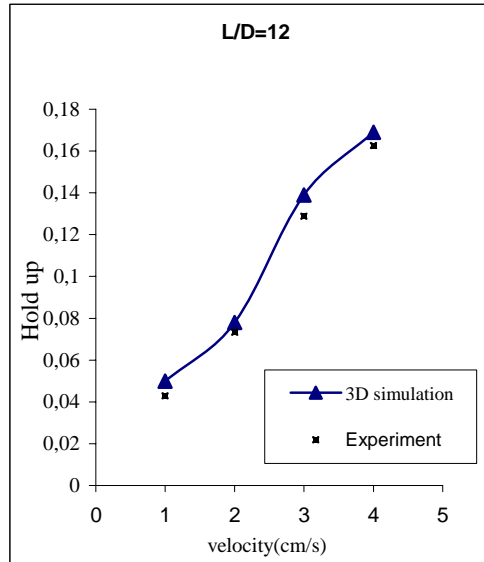

Fig. 13.Comparison of 3D and experiment gas holdup

Full three-dimensional simulations confirmed the major trends observed in two-dimensional simulations (figures 14, 15 and 16). Predicted values of gas volume fraction vary almost linearly with superficial velocity, which is in agreement with the reported data of Haque et al. (1986) [15].
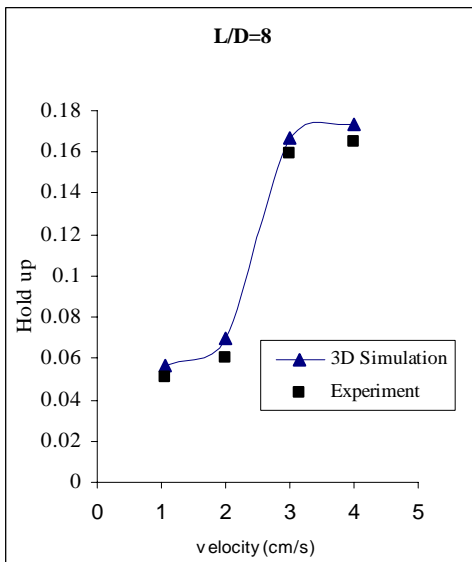

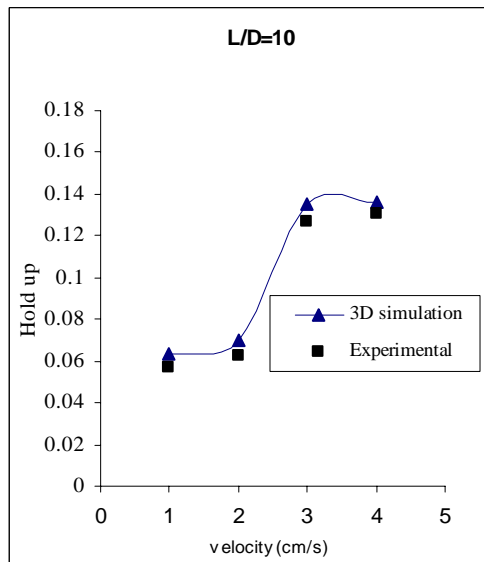Fig.14. Comparison of 3D and experiment gas holdup

Fig 15. Comparison of 3D and experiment gas holdup

In order to ensure the solution independency from the grid size, the geometry was meshed using three different grid sizes and the predicted averaged gas hold up was compared. Table 1 shows the calculated averaged gas hold up using different mesh sizes.

Fine grid captured some of the small-scale flow features which were unable to be detected in simulations with coarser computational cells. According to Table 1, due to the finer grids in the Grid 2 setup, the calculated averaged gas hold up is approximately 15% bigger than the Grid 1 setup. However, the values of calculated averaged gas hold up using the Grids 2 and 3 setups are quite close. In the other words, no significant changes were observed in the predicted averaged gas hold up for the Grid 3 setup when it is compared with that predicted for the Grid 2 layout. Therefore, the Grid 2 setup was chosen due to the lower required computation time. In this mesh configuration, the domain was divided into 194304 numbers of tetrahedral cells.

Table1. Effect of grid size (3D)

	No. of cells	ε_g
Grid1	24288	0.0847
Grid2	194304	0.1213
Grid3	242888	0.1254

This indeed shows that the number of computational cells used in the first 3D simulation was large enough to simulate the exact hydrodynamic behavior of the system. The real time of steady state point was predicted in 3D case correctly which was agreed with experimental very well (250 sec). The contours of velocity for some cross sections of column show that axisymmetric guess not valid for bubble column (Figure 16).

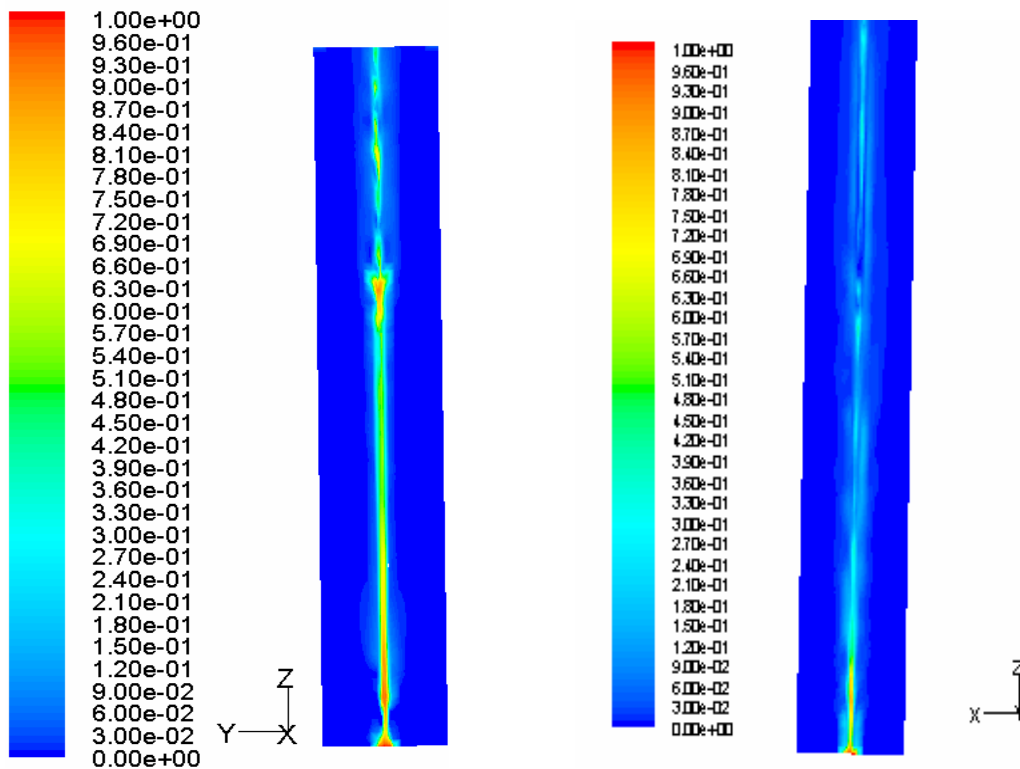Figure.16 contour of gas volume fraction in different cross section for 3D case

6. Conclusion

The hydrodynamic simulation of the bubbly flow in a cylindrical laboratory-scale bubble column was carried out successfully with a commercial CFD package. An Eulerian-Eulerian two-phase flow model is applied including a $k - \varepsilon$ turbulence model. The simulations are validated with experimental data for gas hold-up.

If the 2D laminar model is applied for calculations, the simulation results depend strongly on the space resolution used. The finer the space grid the more vortices are resolved, in accordance with the turbulent character of the underlying flow.

If the 2D k-ε turbulence model was used instead, the value of the effective viscosity was overestimated by one order of magnitude, and the transient characteristic of the flow was dampened out in the calculation. As the three-dimensional results show, the 2D turbulent model is not capable of reproducing the dynamic characteristics of the flow, due to the fact, that the column walls dampens the turbulence intensity which results in a decrease of the effective viscosity inside the apparatus. The results obtained with the 3D version of the k-ε turbulence model are on the contrary in surprisingly good qualitative and acceptable quantitative agreement with experimental results.

The inclusion of the standard $k - \varepsilon$ turbulence model is, however, useful to describe the instantaneous large-scale vertical flow   structure correctly.

Laminar simulations also do not reproduce the behavior of the test case, and a turbulence model has to be considered. Further research in the area of CFD modeling of gas-liquid flows is strongly necessary to understand in detail all the phenomena taking place in a bubble column reactor.

Nomenclature

P	pressure
$\bar{v}$	velocity vector
S_{pq}	rate of mass transfer between p and q phases
ρ_q	phase density
μ_q	viscosity phase q
μ	viscosity of mixture phases
α_q	volume fraction of each phase
D	column diameter
L	column length
$\dot{m}_{pq}$	interphase mass transfer
K	turbulent kinetic energy
ε	turbulent kinetic energy dissipation rate
G_b	turbulence equation parameter
G_k	turbulence equation parameter

References

[1] Becker, S., Sokolichin, A., Eigenberger, G.: (1994). Gas-liquid flow in bubble columns and loop reactors: Part II. ,"Comparison of detailed experiments and flow simulations" Chemical Engineering Science, 49(24B), 5747-5762.

[2] Shah, Y. T.: (1979). "Gas–liquid–solid reactor design", New York: McGraw-Hill.

[3] Delnoij, E., Lemmers, F.A., Kuipers, J.A.M., van Swaaij, W.P.M.: (1997). "Dynamic simulation of dispersed gas-liquid two-phase flow using a discrete bubble model" Chem. Engng Sci., 52, 1429-1458.

[4] Sokolichin, A., Eigenberger, G., Lapin, A., Lukbbert, A.: (1997)" Dynamic numerical simulation of gas-liquid two-phase flows Euler-Euler versus Euler-Lagrange", Chem. Eng Sci., 52, 611-626.

[5] Ranade, V. V.: (1993). Numerical simulation of turbulent flow in bubble column reactors. A.I.Ch.E. Symposium Series, 89(293), 61-71.

[6] Lapin, A., Lukbbert, A.: (1994). Numerical simulation of the dynamics of two-phase gas-liquid flows in bubble columns. Chemical Engineering Science, 49(21), 3661-3674.

[7] Devanathan, N., Dudukovic, M., Lapin, P. A., & Lubbert, A.: (1995), "Chaotic flow in bubble column reactors", Chemical Engineering Science, 50, 2661-2667.

[8] Delnoij, E., Lemmers, F.A., Kuipers, J.A.M., & van Swaaij, W.P.M.: (1997), "Dynamic simulation of dispersed gas-liquid two-phase flow using a discrete bubble model", Chem. Eng Sci., 52, 1429-1458.

[9] Becker, S., Sokolichin, A., Eigenberger, G.: (1994). Gas-liquid flow in bubble columns and loop reactors: Part II. Comparison of detailed experiments and flow simulations. Chemical Engineering Science, 49, 5747-5762.

[10] Torvik, R., Svendsen, H. F.: (1990)," Modelling of slurry reactors: A fundamental approach", Chemical Engineering Science, 45, 2325-2332.

[11] Svendsen, H. F., Jakobsen, H. A., Torvik, R.: (1992). Local flow structures in internal loop and bubble column reactors. Chemical Engineering Science, 47, 3297-3304.

[12] Jakobsen, H. A., Sannaes, B. H., Grevskott, S., Svendsen, H. F.: (1997)"Modelling of vertical bubble-driven flows", Industrial Engineering Chemical Research, 36, 4052-4074.

[13] Grevskott, S., Sannes, B. H., Dudukovic, M. P., Hjarbo, K. W., Svendsen, H. F.: (1996). "Liquid circulation, bubble size distributions, and solids movement in two and three-phase bubble columns", Chemical Engineering Science, 51, 1703-1723.

[13] Ranade, V. V.: (1997), "Modelling of turbulent flow in a bubble column reactor", Chemical Engineering Research and Design, 75, 14-23.

[14] Sokolichin, A., Eigenberger, G., Lapin, A., Lubbert, A.: (1997)," Dynamic numerical simulation of gas-liquid two-phase flows: Euler-Euler versus Euler-Lagrange. Chem. Engng Sci., 52, 611-626.

[15] Haque, M.W., Nigam, K.D.P., Viswanathan, K., Joshi, J.B. : (1988) Studies on bubble rise velocity in bubble columns employing non-Newtonian solutions, Chemical Engineering Communications 73 31–42.